Theoretical Study of Reaction Mechanisms of OH Radical with Toluene 1,2-Epoxide/2-Methyloxepin

Rocío Cartas-Rosado[†] and Miguel Castro*

Facultad de Química, Departamento de Física y Química Teórica Universidad Nacional Autónoma de México, D. F. 04510, México

Received: June 28, 2007; In Final Form: October 2, 2007

In this study, the reaction mechanism of toluene 1,2-epoxide/2-methyloxepin with OH radical was studied by means of quantum chemical computations performed using B3LYP/6-31G(d,p), B3LYP/6-311G(2df,2p), and BHandHLYP/6-31G(d,p) methods. Ground state, intermediate, and transition states were determined. The results indicated that the 2-methyloxepin, **A**, isomer is more stable, by 2.4 kcal/mol, than toluene 1,2-epoxide, **B**. Two reaction pathways were studied, **RP-A** and **RP-B,** corresponding to the reaction of OH with toluene 1,2-epoxide and 2-methyloxepin, respectively. The localization of a pre-reactive complex for **RP-A** is crucial for the accurate estimation of the rate constant, $k = 1.0 \times 10^{-10}$ cm^3 molecule^{-1} s^{-1}, which is in good agreement with that determined experimentally, whereas for **RP-B** the rate constant is 1.3×10^{-14} cm^3 molecule^{-1} s^{-1}. Under atmospheric conditions, both pathways yield 6-oxohepta-2,4-dienal as a main product, and from the energetic and kinetic results it was found that **RP-A** is the preferred pathway. The study of the oxide/oxepin mechanism is relevant because, aside from its relatively high concentration in the troposphere, this compound has carcinogenic and mutagenic properties.

1. Introduction

Volatile organic compounds (VOC) are emitted in substantial quantities from both biogenic and anthropogenic sources[1a,b] and have a major influence on the chemical composition of the atmosphere at the level of lower atmosphere or troposphere. Certain oxidized organic products with low volatility can remain at the level of troposphere and can promote both aerosol formation and growth of these aggregates.[2] The important contribution of such primary oxygenated organics to secondary organic aerosols (SOA) is becoming increasingly recognized.[3] Nowadays, there has been some evidence that SOA may affect human health and global warming. In fact, the probable formation of toxic epoxide species from aromatic oxidation is of paramount importance, because the epoxy functional group can act as an electrophile in its interaction with DNA and nucleosides, producing carcinogenic and mutagenic damages.[4]

Aromatic hydrocarbons constitute the largest fraction, 20%, of VOCs in polluted atmosphere in urban areas,[5] with anthropogenic activities being their main source of origin. Toluene is the most abundant aromatic hydrocarbon in the troposphere; during the day, the main loss process is the gas-phase reaction of this aromatic compound with the OH radical. Theoretical studies have been realized to investigate the preferential position for the primary addition of the OH radical.[6,7] Within the framework of density functional theory (DFT), Inseon et al.[6] using the B3LYP/6-31G(d,p) method determined a preferential position for the *ortho* addition of OH to toluene. Whereas Uc et al.,[7] using Hartree−Fock theory at the PMP2 level, concluded that the *ipso* addition of OH to toluene is the most important. In particular, the *ortho* addition yields a radical intermediate, which is oxidized by molecular oxygen to toluene 1,2-epoxide and 2-methyloxepin; a rapid equilibrium was observed for these species,[8a] which have both toxic and mutagenic properties.[4]

The mechanisms for the reaction of toluene 1,2-epoxide/2-methyloxepin with the OH and NO_3 radicals were proposed by Klotz et al.[8a] For the reaction with OH, these authors obtained a rate constant of $(2.1 \pm 0.1) \times 10^{-10}$ cm^3 molecule^{-1} s^{-1} and 6-oxohepta-2,4-dienal was identified as the final product. They also found that the reaction with the NO_3 radical proceeded with a rate constant of $(1.3 \pm 0.1) \times 10^{-11}$ cm^3 molecule^{-1} s^{-1} and that the main products were unidentified nitrogen-containing compounds. Besides, other authors have proposed the formation of *m*-xylene oxide/oxepin to explain the formation of the observed 2-methyl-6-oxo-2,4-heptadienal and 4-methyl-6-oxo-2,4-hexadienal species as final products.[9] On the other hand, Kassaee et al.,[10] by means of an *ab initio* Hammet study, have determined the substituent effects on the tautomerization of oxepine to benzene oxide. They concluded that electron-withdrawing groups shift the equilibrium slightly in favor of benzene oxide. Raoult et al.[11a,b] have determined experimentally and theoretically the primary oxidation steps of benzene + OH in the gas phase. Using B3LYP/6-31G(d) and single point CCSD(T)/6-31G(d)//B3LYP/6-31G(d) calculations, these authors pointed out that near atmospheric conditions, the O_2 addition to the benzene−OH intermediate is in equilibrium with the corresponding peroxy radical (ROO), which, despite the possible reaction routes with high activation barriers, forms glyoxal as a primary product. Whereas Frankcombe et al.,[12] using the B3LYP/6-311G(2df,2pd) method, have studied the toluene−OH−O_2 system following the proposal of oxide/oxepin mechanisms by Klotz et al.[8a] and found that the hydrogen abstraction by O_2, leading to the formation of the toluene oxides, presents barriers of ≅9.6 kcal/mol, with respect to the energy of the toluene entrance channel.

Even though the carcinogenic and mutagenic properties of the oxide/oxepin system are known, there are few experimental

* Corresponding author. E-mail: castro@quetzal.pquim.unam.mx.
[†] On a postdoctoral stay at the Facultad de Química, UNAM.

10.1021/jp075052q CCC: $37.00 © 2007 American Chemical Society
Published on Web 11/29/2007

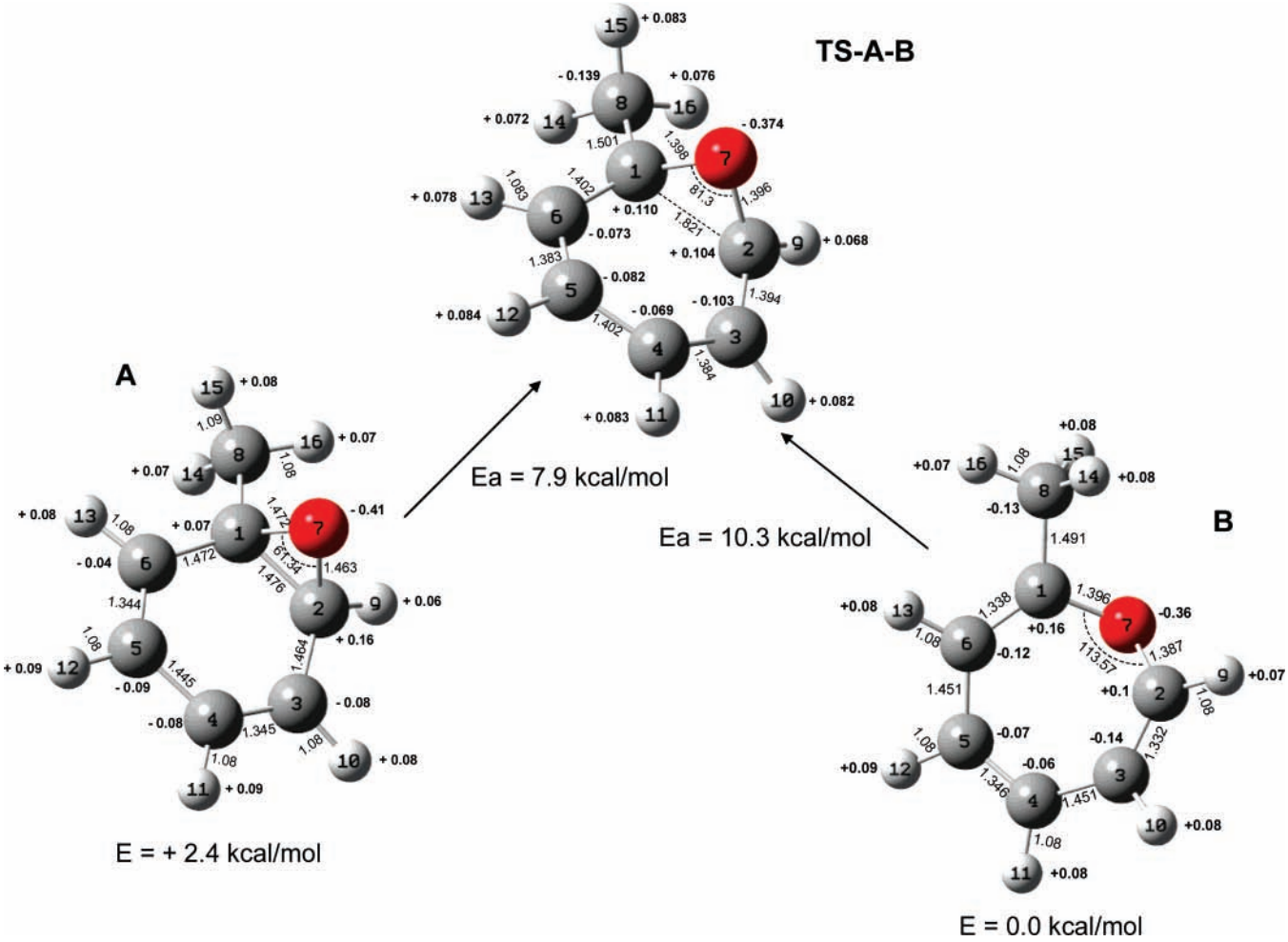

Figure 1. B3LYP/6-311G(2df,2p) optimized structure of toluene 1,2-oxide/2-methyloxepin (**A**/**B**). The transition state structure is also indicated.

TABLE 1: IR Stretching Vibration of A and B Calculated at the B3LYP Level with 6-31G(d,p) and 6-311G(2df,2p) Basis Sets

	toluene 1,2-oxide (**A**)		2-methyloxepin (**B**)		
stretching (cm^{-1})	B3LYP 6-311G(2df,2p)	B3LYP 6-31G(d,p)	B3LYP 6-311G(2df,2p)	B3LYP 6-31G(d,p)	experimental[a]
C−H (vinylic)	3153	3171	3141	3157	3050
C−H (methyl group symmetric)	3034	3046	3027	3038	3000
C−H (methyl group asymmetric)	3090	3112	3121	3140	3000
C═C symmetric	1689	1702	1633	1647	1600
C═C asymmetric	1602	1618	1710	1722	
C−O (epoxide)	1307−1377	1316−1385			
C−O (oxepin)			1258	1260	1235
C−O (oxepin)			1164	1171	1157
C−O (epoxide or oxepin)	1075	1080	1089	1070	1074
C−O (epoxide or oxepin)	1008	1011	1063	1064	1047

[a] As assigned in ref 8a.

and theoretical studies[8a,b,10,12,13] of these compounds. In this study, investigations are particularly performed on the structural, electronic, andenergetic properties of toluene 1,2-oxide and 2-methyloxepin at the B3LYP/6-31G(d,p), B3LYP/6-311G(2df,-2p), and BHandHLYP/6-31G(d,p) levels of theory. The calculated vibrational frequencies were compared with the experimental FT-IR spectrum[8a] of toluene 1,2-oxide/2-methyloxepin. As shown below, the present results indicate that BHandHLYP/6-31G(d,p) is an appropriate method for the analysis of these kind of compounds. We have investigated several possibilities for the OH radical addition to toluene 1,2-epoxide/2-methyloxepin and determined the corresponding transition state that connects the reactants with each organic compound. An important feature of the theoretical results is based on the fact that these two isomers have nearly similar energies, thereby complicating the analysis of their reactivity. The estimation of the rate constant using the BHandHLYP/6-31G(d,p) method indicates that the reaction of OH + toluene 1,2-epoxide dominates over the OH + 2-methyloxepin pathway in the atmospheric chemistry.

Also, we report the potential energy surface (PES) for the mechanism of OH + toluene 1,2-oxide (**RP-A**) and OH + 2-methyloxepin (**RP-B**). Both pathways produce 6-oxohepta-2,4-dienal as one of the main final product. The activation energy (E_a) and the reaction energy (RE, calculated as the difference between two contiguous intermediates) were evalu-

SCHEME 1

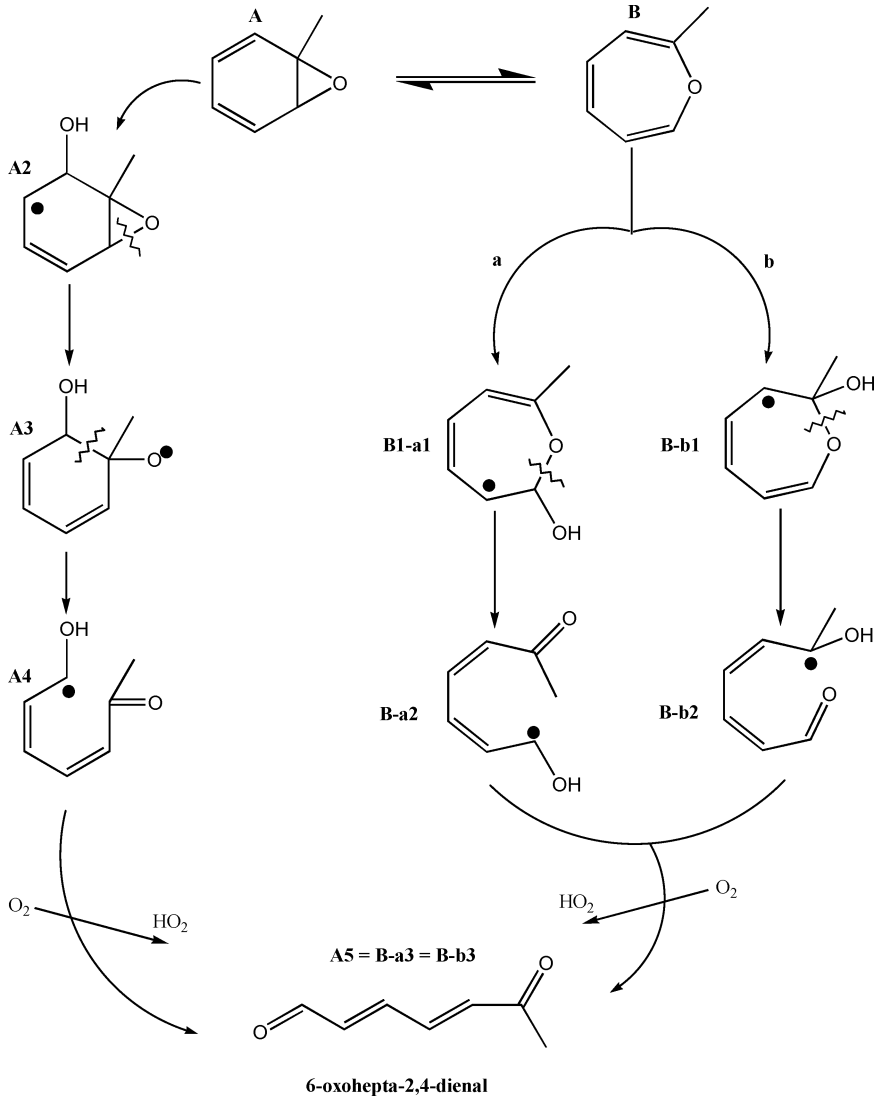

TABLE 2: Zero-Point Corrected Reaction Energies (RE, kcal/mol) and Activation Energies (E_a, kcal/mol) for Toluene 1,2-Oxide−OH Reaction Mechanism for Reaction Pathway A

	reaction pathway **A**					
	B3LYP/6-31G(d,p)		B3LYP/6-311(2df,2p)		BHandHLYP/6-31G(d,p)	
	RE	E_a	RE	E_a	RE	E_a
reactants → **P−C**					−6.41	
P−C → TS-A						2.25
A → A2	−41.63		−40.1		−40.86	
TS-A2_A3		9.41		9.1		11.3
A2 → A3	−31.85		−30.65		−31.23	
TS-A3_A4		6.03		4.8		12.17
A3 → A4 + O2	−28.33		−31.26		−23.37	
TS-A4_A5		−44.47		−41.7		−37.7
A4 → A5	−38.46		−38.12		−39.94	

ated, which allow us to verify whether the proposed channel to yield 6-oxohepta-2,4-dienal is energetically favorable. Understanding the atmospheric oxidation of aromatic hydrocarbons is needed for an insight into such kind of reactions and for an improvement in the predictions of the model calculations.

2. Computational Procedure

The geometry and electronic structure of all compounds studied in this work were determined by means of calculations carried out in the spin-restricted and the spin-unrestricted formalisms for closed-shell and open-shell systems, respectively. We performed geometry optimizations using three different electronic structure approaches of hybrid density functional theory (HDFT).

At the HDFT level, the B3LYP hybrid functional was used. B3LYP is the combination of Becke's three-parameter exchange functional, and the correlation is provided by the Lee, Yang, and Parr expression (LYP) functional. This hybrid scheme was used in conjunction with the split valence polarized basis sets, 6-31G(d,p) and 6-311G(2df,2p). Several authors have already

TABLE 3: Partition Functions Q_{corr}[a] and Pre-exponential Factors *A* for Paths A (Toluene 1,2-Oxide) and B (2-Methyloxepin) for Complex Mechanism of the OH Addition Reaction, Calculated at the BHandHLYP/6-31G(d,p) Level (Experimental Rate Constant (2.1 ± 0.1) × 10^{-10} [8])

	toluene 1,2-oxide **A** (no elemental reaction)		2-methyloxepin **B** (elemental reaction)
Q_{OH}	5.99913×10^{7}	Q_{OH}	5.99913×10^{7}
Q_{A}	8.39202×10^{13}	Q_{B}	1.68144×10^{14}
Q_{Acorr}	1.0325790×10^{13}	Q_{Bcorr}	6.88×10^{12}
Q_{P-C}	2.86414×10^{16}		
$Q_{P-Ccorr}$	2.73943×10^{16}		
Q_{TS}	1.95399×10^{15}	Q_{TS}	5.55473×10^{14}
Q_{TScorr}	5.56648×10^{15}	Q_{TScorr}	1.2360×10^{15}
A (cm^3 molecule^{-1} s^{-1})	1.262369 x 10^{12}	A (cm^3 molecule^{-1} s^{-1})	2.538555×10^{7}
K_{eq} (cm^3 molecule^{-1})	3.67×10^{-21}		
k (s^{-1})	2.83×10^{10}		
k_{eff} (cm^3 molecule^{-1} s^{-1})	1.0×10^{-10}	k_{eff} (cm^3 molecule^{-1} s^{-1})	1.3×10^{-14}

[a] The indicated partition functions have been corrected (Q_{corr}) for internal rotations (see text); the other values are those obtained from Gaussian03.

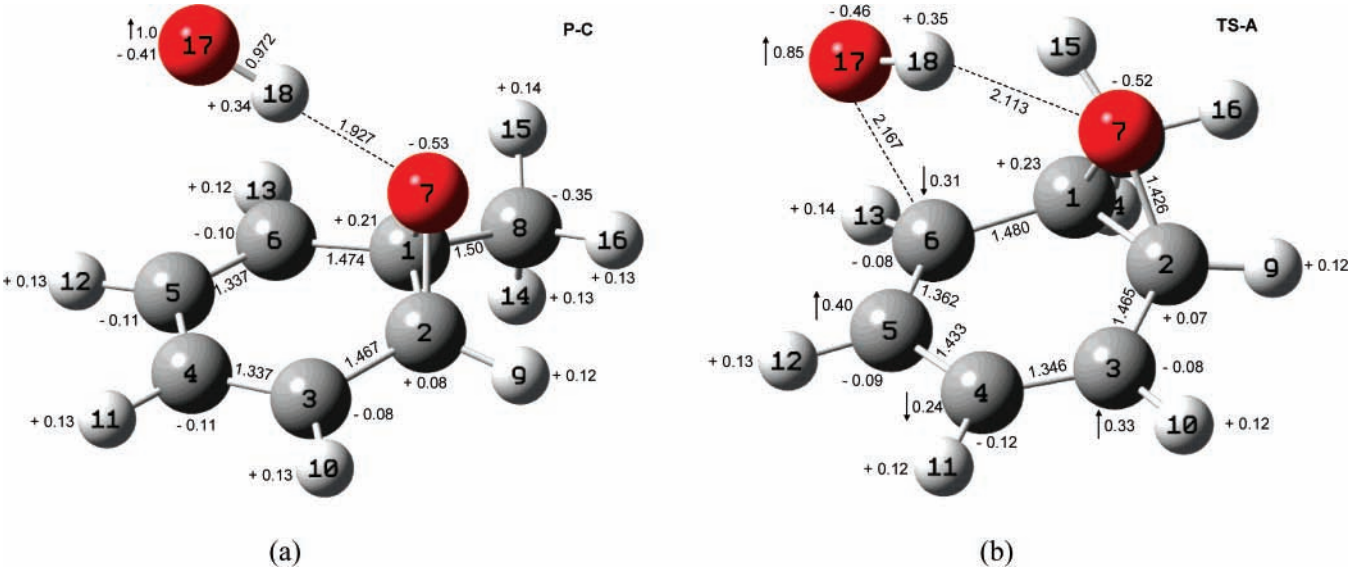

Figure 2. Optimized structure for the pre-reactive complex (a) and transition state (b) for **RP-A** at the BHandHLYP/6-31G(d,p) level of theory.

proved that B3LYP is adequate to describe OH−toluene reactions.[6,7] Similarly, it is also now well-known that B3LYP systematically underestimates barrier heights (particularly, hydrogen-abstraction barriers).[14,15] Thus, other functionals were tested in this work. That is, the PES was also studied using the BH&HLYP functional,[16] because empirically it has been found that this method gives more accurate barrier heights than B3LYP.[14,17] The calculations were realized using the Gaussian (03) program.[18]

The located transition states, TS, were confirmed by means of the analysis for the vibrational frequencies; a single imaginary frequency, defined along the reaction coordinate was presented by such states. The rate constant for the OH addition to oxide/oxepin has been calculated assuming that the reaction occurs according to a two-step mechanism. In the first step, there is a fast pre-equilibrium between the reactants and the pre-reactive complex, and in the second step, the addition of OH radical occurs. Therefore, the equilibrium constant of the fast pre-equilibrium may be obtained as[19a]

First Step: $C_6H_5OCH_3 + OH^{\bullet} \leftrightarrow [C_6H_5OCH_3{-}OH]^{\bullet}$

Second Step: $[C_6H_5OCH_3{-}OH]^{\bullet} \rightarrow C_6H_5OCH_3OH$

In the first step, k_1 and k_{-1} are the rate constants for the forward and reverse reactions, respectively, whereas k_2 is the rate constant for the second step, a steady state analysis origin a rate constant for the overall reaction, which is possibly written as

$$k = \frac{k_1 k_2}{k_{-1}} = \left(\frac{A_1 A_2}{A_{-1}}\right) \exp[-(E_1 + E_2 - E_{-1})/RT] \qquad (1)$$

Because E_1 is zero, the activation energy of the overall reaction is

$$E_a = E_2 - E_1 = (E_{TS} - E_{P-C}) - (E_R - E_{P-C}) = E_{TS} - E_R \qquad (2)$$

where E_R, E_{P-C}, and E_{TS} are the total energy for the reactants, transition state, and pre-reactive complex, respectively. At high pressures, the activation energy can be calculated as eq 2. Then, the constant of the fast equilibrium reaction between the reactants and the pre-reactive complex can be obtained using basic statistical thermodynamic principles

$$K_{eq} = \frac{Q_{P-C}}{Q_R} \exp[(E_R - E_{P-C})/RT] \qquad (3)$$

where Q_R and Q_{P-C} are the partition functions of the reactants and pre-reactive complex, respectively. Under high-pressure conditions, an equilibrium distribution of reactants is maintained

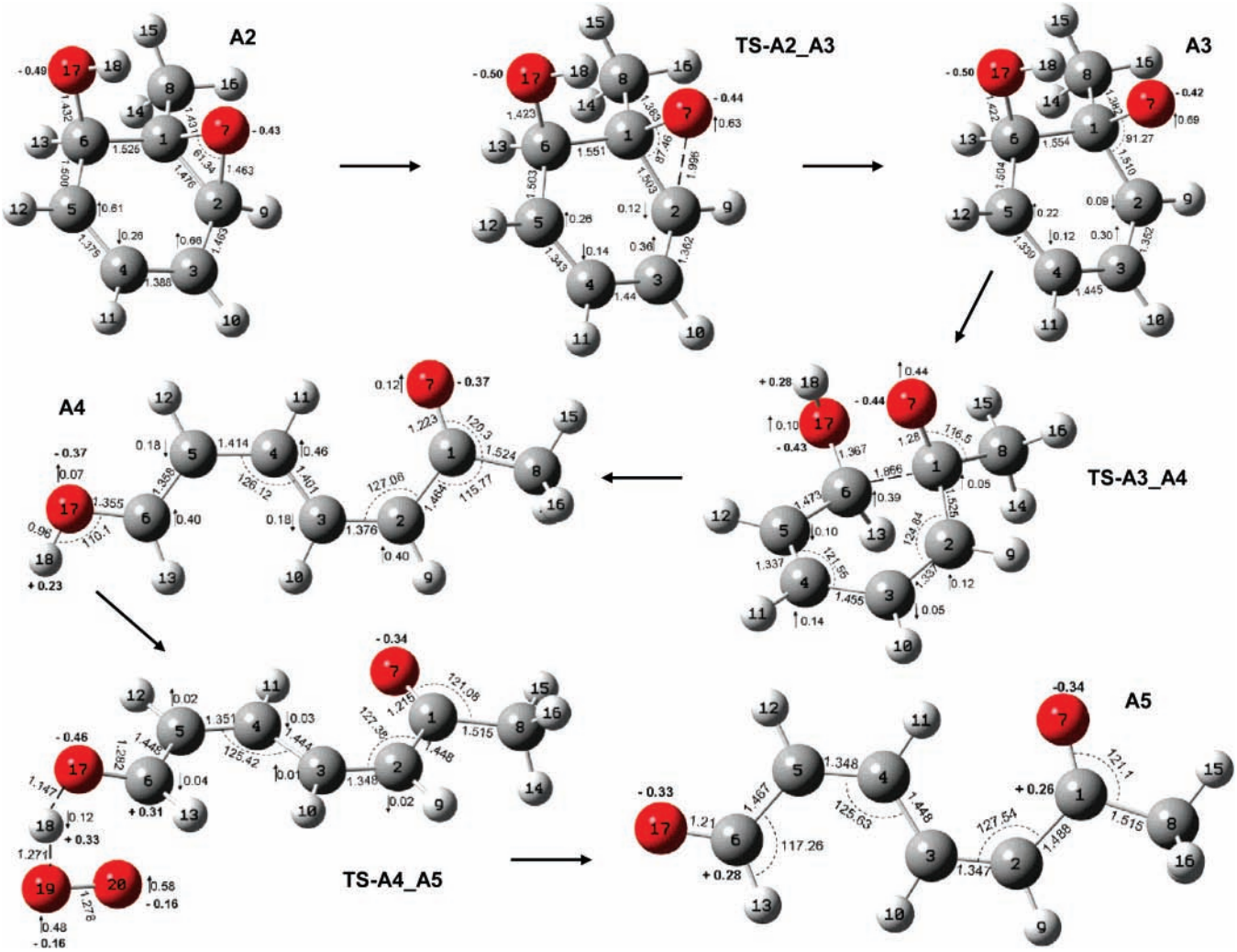

Figure 3. Intermediates and transition states for reaction pathway **A**, at the B3LYP/6-311G(2df,2p) level of theory.

in a unimolecular process, and the classical transition state theory[19b] formula can be used to estimate k.

$$k = \frac{k_B T}{h} \frac{Q_{TS}}{Q_{P-C}} \exp[(E_{P-C} - E_{TS})/RT] \quad (4)$$

Partition functions, Q, are computed from the rotational constants and the vibrational frequencies of the BHandHLYP results. The effective rate constant for the overall mechanism is obtained according to the following equation:

$$k_{effec} = K_{eq} k \quad (5)$$

3. Results and Discussion

The main objective of this study is to explore the potential energy surface (PES) for the oxidation mechanism of toluene 1,2-oxide and 2-methyloxepin to yield 6-oxohepta-2,4-dienal. As mentioned above, calculations were performed using the B3LYP functional and the 6-31G(d,p) and 6-311G(2df,2p) basis sets. The located adducts of lowest energy were re-optimized using the BHandHLYP/6-31G(d,p) method.

The computed B3LYP/6311-G(2df,2p) lowest energy structure of toluene 1,2-oxide **A** and of 2-methyloxepin **B** are shown in Figure 1. For the isomer **A**, the Mulliken population analysis reveals an uneven distribution of the atomic charges. The oxygen atom, with −0.41 electrons (e), is the most negative center, followed by the carbon atom of the methyl group, which has −0.15 e. Other small negative charges appear at C3−C4−C5−C6, which is a consequence of the electronic density from the two double bonds. This atomic net charge distribution produces a dipole moment of 1.82 Debyes (D), indicating a high polarity for toluene 1,2-oxide. Note that this dipole matches that of the water molecule (the calculated dipole moment for H_2O is equal to 1.88 D, at the B3LYP/6311-G(2df,2p) level of theory). In the absence of degradation reactions for **A**, these results suggest a high solubility of this compound in polar solvents. The structural features of 2-methyloxepin (**B**) indicate, as compared to the oxide, a less stressed ring. In fact, the results of total energy indicate that **B** is 2.4 kcal/mol more stable than **A**. The electronic charge in **B** is also unevenly distributed, producing a polar compound, but with a smaller dipole, 1.18 D, than that of **A**; see Figure 1. In addition, we found that the activation energy (E_a) of transition state **TS-A-B** for reaction **A** → **B** is 7.9 kcal/mol, whereas for the inverse reaction **B** → **A**, the E_a is of 10.3 kcal/mol; see Figure 1. These results are in agreement with the observation that the equilibrium is displaced toward the less polar oxepin moiety when the **A**/ **B** system is dissolved in CF_3Br.[20a]

In Table 1, the theoretical frequencies for the optimized **A** and **B** geometries using the B3LYP functional, are compared with the experimental gas-phase FT-IR. The experimental and theoretical values for the stretching vibrations are in close agreement. The FT-IR[8a] spectrum shows absorption at 1235 and 1157 cm^{-1} corresponding to C−O stretching vibrations of vinyl

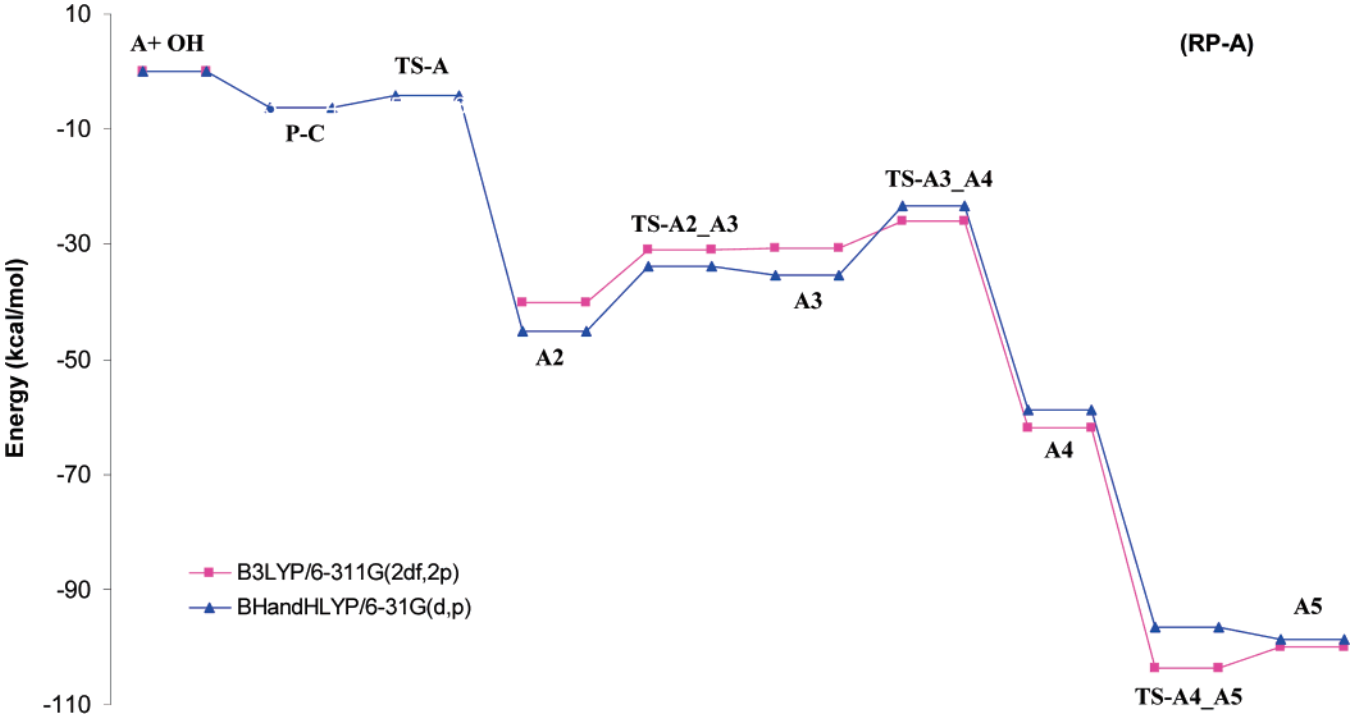

Figure 4. PES, at BHandHLYP/6-31G(d,p) and B3LYP/6-311G(2df,2p), for reaction pathway A (**RP-A**).

ethers or epoxides. The bands at 1074 and 1047 cm^{-1} are also typical regions for vinyl ether. Comparison between the experimental, 1235 and 1157 cm^{-1}, and theoretical, 1258 and 1164 cm^{-1}, frequencies (see Table 1) indicates they can be assigned to the C−O group of **B**. No assignments were made for the absorption at 1300−1390 cm^{-1},[8a] but their calculated counterparts, 1307 and 1377 cm^{-1}, indicate that this absorption corresponds to the C−O stretching of the epoxide **A**. The most intense absorptions in the spectrum[8a] are due to **B**, suggesting that this isomer may be present in higher concentrations than **A**, at 300 K. These results are in agreement with the fact that **B** is more stable than **A**, by 2.4 kcal/mol, and with the **B** → **A** activation energy of 10.3 kcal/mol. The results in Table 1 indicate that the chosen methods, B3LYP/6-311G(2df,2p) and B3LYP/6-31G(d,p), accurately describe the absorption spectrum of toluene 1,2-oxide **A** and of 2-methyloxepin **B.** This analysis helps to distinguish between both isomers.

According to Klotz et al.,[8a] the equilibrium of toluene 1,2-oxide **A** with 2-methyloxepin **B** is of critical importance to their atmospheric chemistry behavior. Gunther et al.[20b] measured the rate constant for the conversion of toluene 1,2-oxide to 2-methyloxepin and found that the equilibrium of these species is established much more rapidly than any conceivable atmospheric degradation reaction. In fact, **A** and **B** have been considered as a single compound, which complicates the analysis of their reactivity. The following text gives the reaction mechanism for both **A** and **B** compounds.

3.1. Reaction Pathway A: Toluene 1,2-Oxide + OH. The addition of the OH radical to the C6 position of **A** produces the **A2** intermediate, shown in Scheme 1. In a primary ring cleavage, **A2** is stabilized, resulting in the formation of the **A3** intermediate, a further cleavage yields **A4**, which, through an abstraction of the H-atom by the O_2 molecule, produces 6-oxohepta-2,4-dienal **A5**. This compound has been experimentally identified as one of the products in the reaction of toluene 1,2-oxide with the OH radical.[8a] The obtained activation energy (E_a) and the reaction energy (RE), at several levels of theory, for the involved species in **RP-A** are shown in Table 2. All necessary parameters for the calculation of the rate constants are given in Table 3. In this study, the rate constants were estimated, considering the barrier for the (a) elemental and (b) nonelemental reactions:

$$\mathbf{R} \rightarrow \mathbf{TS}\ \text{(reactants} \rightarrow \text{transition state)} \qquad \text{(a)}$$

$$\mathbf{R} \rightarrow \mathbf{P{-}C} \rightarrow \mathbf{TS}$$
$$\text{(reactants} \rightarrow \text{pre-reactive complex} \rightarrow \text{transition state)} \qquad \text{(b)}$$

As will be shown below, the nonelemental reaction produces results in close agreement with the experimental determinations.[7,21,22] It is to be highlighted that the **R** → **P**−**C** → **TS** step was evaluated using the BHandHLYP functional, because it was found that it is adequate to obtain more accurate energy barriers.[16,18]

The hydrogen atom of the O−H radical appears to approach a lone pair of the oxygen atom in the toluene 1,2-oxide to form a stable pre-reactive complex (**P**−**C**), and this complex is 6.41 kcal/mol more stable than the energy of the reactants. The oxygen atom of the OH radical may flip in the plane, in the direction of the C6 carbon atom to form a new C6−O bond; see Figure 2a. At this point, we do not use the B3LYP method because it is inherently inadequate to describe some of the bonding interactions presented in different pre-reactive complex structures.[23] This pre-reactive complex will undergo stabilization by collision, dissociation back to reactant, and fragmentation to final product.[24] The existence of a pre-reactive structure was observed by other authors.[21,22] Uc et al.[7] found a pre-reactive structure with energy below that of the reactants for the addition of the OH radical to toluene and concluded that it can be considered as the precursor structure for all further addition reactions.

After the pre-reactive complex formation, the corresponding transition state **TS-A** geometry was obtained at the BHandHLYP/6-31G(d,p) level of theory; see Figure 2b. The activation energy of this transition state is given in Table 2. From the estimated frequencies for **TS-A**, two modes were identified as internal rotations corresponding to rotation of OH and of the

TABLE 4: Zero-Point Corrected Reaction Energies (RE, kcal/mol) and Activation Energies (E_a, kcal/mol) for 2-Methyloxepin + OH Reaction Mechanism for Reaction Pathway B

reaction pathway **B**	pathway **A**						pathway B					
	B3LYP 6-31G(d,p)		B3LYP 6-311(2df,2p)		BHandHLYP 6-31G(d,p)		B3LYP 6-31G(d,p)		B3LYP 6-311(2df,2p)		BHandHLYP 6-31G(d,p)	
	RE	E_a	RE	E_a	RE	E_a	RE	E_a	RE	E_a	RE	E_a
B + OH	0	0	0	0	0	0	**B** + OH	0	0	0	0	0
TS-Bab		−10.7		−9.5		0.97	**TS-Bab**		−10.7		−9.5		0.97
B → B-a1	−54.31		−52.98		−51.91		**B → B-b1**	−53.72		−52.41		−51.6	
TS-a1_a2		12.6		9.8		19.23	**TS-b1_b2**		8.1		7.3		16.5
B-a1 → B-a2	−3.43		−4.89		−0.28		**B-b1 → B-b2**	−9.26		−10.7		−5.18	
TS-a2_a3		−52.5		−41.7		−37.7	**TS-b2_b3**		−40.8		−37.9		−35.16
B-a2 → B-a3	−38.46		−38.13		−39.94		**B-b2 → B-b3**	−33.23		−32.88		−35.35	

methyl group. The calculation of rate constants involves the determination of the correct partition functions, in which the internal rotations, with rotational barriers lower than 3 kcal/mol, are treated as hindered rotations rather than as vibrations. The calculated barriers for the internal rotation of OH and CH_3 are lower than 3 kcal/mol. Thus, in the partition function (Q) for the transition state, their harmonic contributions were corrected and replaced by those of hindered rotors (Q_{corr}).[25] Thus, the pre-reactive complex in **R → P−C → TS** yields an actual activation energy ($E_{\mathbf{R}} - E_{\mathbf{P-C}}$) of 6.41 kcal/mol for the pre-equilibrium and a rate constant of 1.0×10^{-10} cm^3 molecule^{-1} s^{-1}, in good agreement with the experimental results. When we assume an elementary mechanism, **R → TS**, the calculated reaction constant is only 3.5×10^{-11} cm^3 molecule^{-1} s^{-1}.

We explore all the possibilities of addition in **A**, and the results show that the C6 carbon atom is the preferred position for the OH addition, yielding the **A2** intermediate, which is stabilized by 40.1 kcal/mol with respect to **A**. Frankcombe et al. obtained similar results for this step.[12] The OH addition to **A** reduces the C1−C2-O7 bond angle by 2.3° to form a more stressed oxide ring in **A2**. Then, a further reaction may take place at this oxide region. In fact, in the stressed oxide ring, the breaking of the C2−O7 bond occurs with an activation energy of 9.1 kcal/mol (at B3LYP/6-311G(2df,2p) level) to yield the **A3** intermediate. The corresponding transition state **TS-A2_A3** presents only one imaginary frequency with an associated vector involving the C2−O7 bond stretching. In **TS-A2_A3**, the C2−O7 distance increases by 0.533 Å; moreover, the C1−C2 bond is relaxed significantly, from 1.485 to 1.503 Å, whereas the C1−O7 bond length, 1.383 Å, has started to move to a double C−O bond. The spin density of **TS-A2_A3** is located on the C2−C3-C4−C5 chain, with a contribution of 0.63 ↑ on the O7 atom. The distribution of the spin density in the ring indicates an anti-ferromagnetic coupling on the C2−C3-C4−C5 chain; see Figure 3.

The **A3** intermediate is 9.8 kcal/mol, at B3LYP/6-311G(2df,-2p), less stable than the parent **A2** oxide, suggesting that **A3** could revert back to the formation of the **A2** compound, instead of forming another product. This behavior was observed in the case of the B3LYP/6-31G(d,p) and BHandHLYP/6-31G(d,p) methods; see Table 2. Some parameters of the **A3** structure are shown in Figure 3. A typical double bond character is found in C2−C3 (1.358 Å) and C4−C5 (1.345 Å), whereas C3−C4 (1.445 Å) is intermediate between double and single bonds; the remaining C−C bonds show characteristics of single C−C bonds. In the **A3** intermediate, the spin density is mainly located on the O7 atom, suggesting a high reactivity of this oxygen site.

The vibrational analysis for **TS-A3_A4** shows a negative frequency with a vector displacement along the C1−C6 bond, which is the one that is broken during the formation of **A4** from **A3**. Indeed, in **TS-A3_A4**, the C1−C6 bond exhibits a significant increase in length of 0.371 Å. At the same time, the C1−O7 distance decreases from 1.383 Å in **A3** to 1.28 Å, indicating the beginning of the C═O double bond formation. As a consequence of ring opening at C1−C6, the C6−O17 bond length decreases considerably by 0.55 Å.

The **A4** intermediate is significantly more stable, by 31.3 kcal/mol, than the **A3** adduct. Furthermore, we have located the transition state **TS-A4-A5**, connecting **A4** with **A5**, which corresponds to the abstraction of hydrogen, H18, by oxygen. The O17−H18 bond increases in length from 0.96 Å in **A4** to 1.147 Å, and simultaneously the H18−O19 bond begins to form,

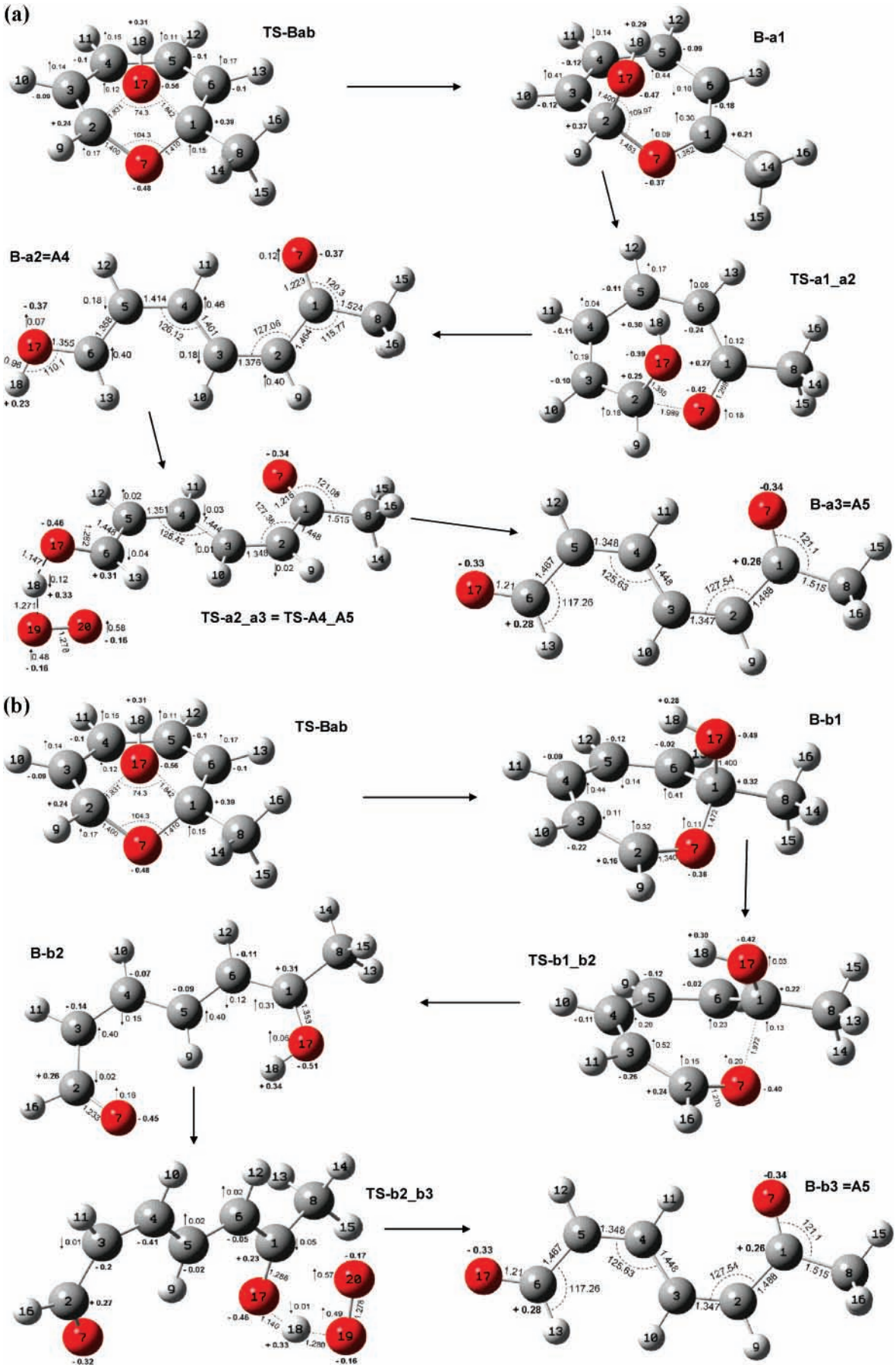

Figure 5. (a) Intermediates and transition states for the reaction pathway **RP-B-a**, at the B3LYP/6-311G(2df,2p) level of theory. (b) Intermediates and transition states for the reaction pathway **RP-B-b**, at the B3LYP/6-311G(2df,2p) level of theory.

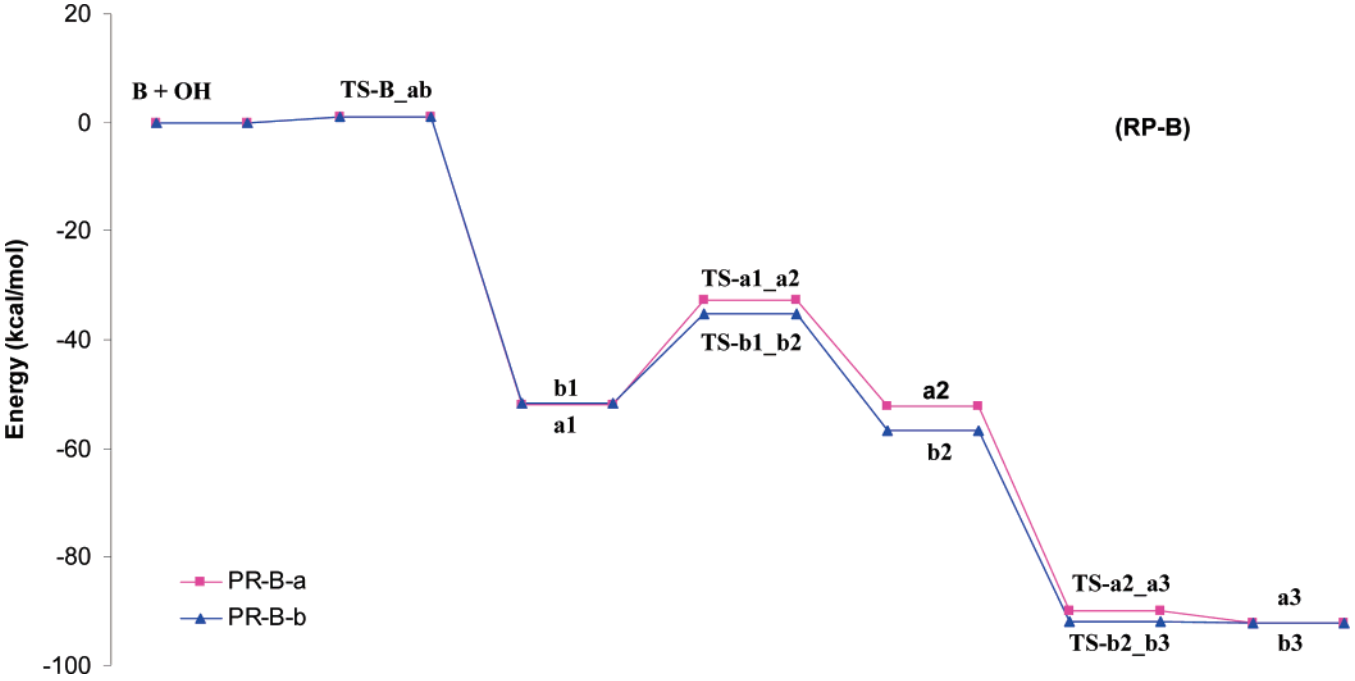

Figure 6. PES, at BHandHLYP/6-31G(d,p) for the reaction pathway **B** (**RP-B**).

with an internuclear distance of 1.255 Å; see Figure 2. Consistently, the spin density of this transition state is mainly localized on the O20 (0.58 ↑), O19 (0.48 ↑), and H18 (0.12 ↑) centers. Finally, abstraction of the H18 acidic hydrogen gives the formation of 6-oxohepta-2,4-dienal, **A5**. It is interesting to note in Table 2 that the B3LYP/6-311G(2df,2p) results present lower activation energies than the other two methods, but only BHandHLYP gives the more stable final product (**A5**). Figure 4 shows the computed BHandHLYP/6-31G(d,p) and B3LYP/6-311G(2df,2p) PES for this reaction pathway **RP-A**.

3.2. Reaction Pathway B: 2-Methyloxepin + OH. This **RP-B** pathway originates two routes: the first one, **B-a**, begins with the addition of the OH radical at the C2 atom, and in the other route, **B-b**, the OH addition occurs at the C1 atom. The total energies for all species, at different levels of theory, are shown in Table 4. The B3LYP/6-311G(2df,2p) optimized structures for **B-a** and **B-b** are shown in Figure 5a,b, respectively.

The B3LYP/6-311G(2df,2p) calculations show the localization of a **TS-Bab** transition state, which presents only one imaginary frequency of 736 cm^{-1}. The **TS-Bab** indicates two possible paths for the OH addition, and it can occur on C2 to give **B-a**, or on C1 to give the **B-b** pathway. This result was confirmed by an internal reaction coordinate (IRC) calculation. The OH addition has no preference for C1 or C2, which may be partially due to the charge distribution of 2-methyloxepin (**B**), as in this moiety, both C1 and C2 have similar positive charges: +0.16 and +0.10 e, respectively. In **TS-Bab**, the C1 and C2 centers become more positive, +0.39 e and +0.24 e, respectively, which is due to the transference of electronic charge toward the O7 and O17 atoms. Note that the C1−O17 and C2−O17 internuclear distances are quite similar, 1.842−1.831 Å. Moreover, the unpaired electron, originated from the OH radical, has been almost completely transferred to 2-methyloxepin, showing a delocalization around the ring.

The rate constant is estimated assuming an elementary reaction. As a matter of fact, for the elementary **R** → **TS** mechanism, the rate constant calculated using the BHandHLYP/6-31G(d,p) method is only 1.3×10^{-14} cm^3 $molecule^{-1}$ s^{-1}. This value is significantly lower than the rate constant of **A**. Moreover, the pre-exponential (*A*) factors for the **A** and **B** channels were calculated using the partition functions derived from the frequency calculations using the BHandHLYP method. The following *A* values were obtained: 1.26×10^{12} cm^3 $molecule^{-1}$ s^{-1} for oxide and 2.54×10^{7} cm^3 $molecule^{-1}$ s^{-1} for oxepin. It is interesting to note the large difference in the pre-exponential factors between these two channels. Thus, the small activation energies for **B** (**R** → **TS-B_ab**), of 0.97 kcal/mol, is expected to compensate for the small value for *A* in the final evaluation of "*k*" through the Arrhenius equation. The obtained values of *k* for **A** (1.0×10^{-10} cm^3 $molecule^{-1}$ s^{-1}) and **B** (1.3×10^{-14} cm^3 $molecule^{-1}$ s^{-1}) suggest that pathway **A** is the dominant reaction. Note that the addition of these *k* values matches the *k* value determined experimentally ($2.1 \pm 0.1) \times 10^{-10}$ cm^3 $molecule^{-1}$ s^{-1}. Nevertheless, differences in reactivity have been observed in the measured concentration−time profiles for benzene oxide/oxepin.[8a] Klotz et al.[8a] pointed out that it is difficult to state which pathway might be dominant; considering the estimations for *k*, we may suggest that the pathway **A**, dominates over pathway **B**.

B-a. Addition of the OH radical to the C2 carbon atom yields the **B-a1** compound, which shows a stabilization energy, with respect to **B**, of 52.98 kcal/mol. Consequently, the C2−C3 double bound in **B** disappears, and the unpaired electron is now mainly localized on the C5 site, with a spin density population of ↑ 0.44.

The breaking of the C−O bond produces the **B-a2** adduct, which is the same as that obtained in the route **A**, and this feature can be clearly appreciated in the **TS-a1_a2** structure shown in Figure 5a. The **TS-a1_a2** transition state yields an activation energy of 9.8 kcal/mol and the C2−O7 distance increases from 1.453 to 1.989 Å, whereas the bond distances of the C2−O17 and C1−O7 bonds decrease. In this transition state, the C2−C3-C4−C5-C6−C1 chain equally shares the spin density; in all these C atoms the spin occurs along the same direction.

The **B-a2** adduct radical is formed from **TS-a1_a2**, joining the routes **A** and **B** at this point; see Figure 5a. The activation energy, involved in the rupture of the C−C bond of **A3**, is lower

than the required value for the C−O bond breaking in **B-a1**; see Table 3, suggesting that route **A** is more favorable for the formation of the same **A3** or **B-a2** compound. Finally, a proton abstraction by the O_2 molecule yields the principal product 6-oxohepta-2,4-dienal. As in route **A**, only the BHandHLYP method locates the product **B-a3** below **TS-a2_a3**; see PES in Figure 6.

B-b. The OH addition to the C1 atom results in the formation of the **B-b1** intermediate; some parameters of this state are given in Figure 5b. The total spin density distribution reveals values of approximately 0.44 and 0.41 for C4 and C6, respectively, indicating the formation of delocalized double bonds in a resonant structure involving the C4−C6 region.

The **TS-b1_b2** structure for the C1−O7 rupture is shown in Figure 5b. The C1−O7 distance, 1.972 Å, is 0.5 Å longer than the corresponding value in the **B-b1** adduct. The activation energies are shown in Table 4. Note that the three methods indicate activation energies for this pathway lower than those of **B-a**. These results predict that the **B-b** route could have a major contribution to the formation of 6-oxohepta-2,4-dienal than the **B-a** route.

As C1−O7 is broken, the **B-b2** intermediate is formed; see Figure 5b. The **B-b2** intermediate is stabilized by 10.7 kcal/mol with respect to **B-b1**. Moreover, as shown in the PES, Figure 6, the **B-b2** intermediate is more stable than its **B-a2** counterpart of the **B-a** pathway. This is probably due to the donor effect of the methyl group adjunct to C1 in **B-b2**. Examination of the atomic charges shows that H18 is the most acid hydrogen atom. The spin density reveals values of ↑ 0.4 for C3 and C5, suggesting that the double bond is delocalized on these carbon atoms. Under atmospheric conditions, the next step is the abstraction of H18 by O_2. The corresponding transition state **TS-b2_b3** is shown in Figure 5b. A negative activation energy was obtained for this abstraction; with a lowest value of 37.9 kcal/mol, at B3LYP/6-311G(2df,2p). The geometry indicates that the O17−H18 bond length is increased by 0.17 Å, whereas the new H18−O19 bond distance is 1.28 Å. Finally, the abstraction of H18 by the O_2 molecule produces the 6-oxohepta-2,4-dienal compound. The results shown in Tables 3 and 4 indicate that only in the BHandHLYP method is a final product produced that is more stable than its corresponding transition state. Overall, the estimated activation energies for **RP-B-b** and **RP-B-a** revealed that the C−O dissociation is the rate-determining step.

4. Conclusions

Reaction mechanisms for the addition of the OH radical to toluene 1,2-epoxide/2-methyloxepin were studied using the B3LYP/6-31G(d,p), B3LYP/6-311G(2df,2p), and BHandHLYP/6-31G(d,p) methods. The obtained results indicate that these two species are quasi-degenerate, because the 2-methyloxepin (**B**) isomer is more stable by only 2.4 kcal/mol. The B3LYP/6-311G(2df,2p) method accurately reproduces the determined vibrational modes of the toluene 1,2-epoxide and 2-methyloxepin compounds. The unambiguous assignments of the calculated signals at 1307 and 1377 cm^{-1} for **A** and at 1258 and 1164 cm^{-1} for **B** help differentiate between these isomers. The rate constant was estimated for two reactions pathways:

RP-A: toluene 1,2-epoxide + OH

$$k = 1.0 \times 10^{-10}\ cm^3\ molecule^{-1}\ s^{-1}$$

RP-B: 2-methyloxepin + OH

$$k = 1.3 \times 10^{-14}\ cm^3\ molecule^{-1}\ s^{-1}$$

The reaction **RP-A** is not elemental, and the overall pathway involves a pre-reactive complex. According to the results for these rate constants, it can be concluded that the dominant reaction is **RP-A**. Even more, a complete (intermediate, pre-reactive complex, transitions states, and the involved energetic properties) mechanism for the formation of the 6-oxohepta-2,4-dienal compound was characterized. We also concluded that 6-oxohepta-2,4-dienal mainly originated from the **RP-A** pathway, because this channel requires a smaller amount of energy to break the C−C bond than that is required for C−O breaking in the **RP-B** pathway. This C−C breaking is accomplished in **RP-A** by the charge-transfer effect of the methyl group adjacent to this bond. Moreover, although the **RP-B** pathway has fewer reaction steps, their activation energies are higher than those of reaction pathway **A**, as indicated by the three methods used in this work. Nevertheless, both routes are complementary to get the right balance of carbons atoms. It was found that only BHandHLYP/6-31G(d,p) predicts that the 6-oxohepta-2,4-dienal is a stable compound. This study allows for a deeper understanding of the reaction mechanism during the oxidation of toluene 1,2-epoxide/2-methyloxepin in urban atmospheres.

Acknowledgment. R. Cartas deeply acknowledges a postdoctoral fellowship from DGAPA, UNAM. We appreciate financial support from Project PAPIIT IN-107905, DGAPA-UNAM, and express our thanks for access to the supercomputer KanBalam at DGSCA-UNAM.

References and Notes

(1) (a) Guenther, A.; Hewitt, C. N.; Erickson, D.; Fall, R.; Geron, C.; Graedel, T.; Harley, P.; Klinger, L.; Lerdau, M.ep McKay, W. A.; Pierce, T.; Scholes, B.; Steinbrecher, R.; Tallamraju, R.; Taylor, J.; Zimmerman, P. *J. Geophys. Res*. **1995**, *100*, 8873. (b) Atkinson, R.; Arey, J. *Chem. Rev.* **2003**, *103*, 4605.

(2) Asher, W. E.; Pankow, J. F.; Erdakos, G. B.; Seinfeld, J. H. *Atmos. Environ.* **2002**, *36*, 1483.

(3) Saxena, P.; Hildemman, L. M. *J. Atmos. Chem*. **1995**, 24, 57.

(4) (a) Ehremberg, L.; Hussain, S. *Mutat. Res.* **1981**, 86, 1. (b) Hemminki, K. *Arch. Toxicol*. **1983**, *52*, 249.

(5) Seinfield, J. H.; Pandis, S. N. *Atmospheric Chemistry and Physics: From Air Pollution to Climate Change*; Wiley: New York, 1997.

(6) Suh, I.; Zhang, D.; Zhang R.; Molina, Luisa T.; Molina, Mario. *Chem. Phys. Lett*. **2002**, *364*, 454.

(7) Uc, V. H.; García-Cruz, I.; Hernandez-Laguna; Vivier-Bunge, A. *J. Phys. Chem*. **2000**, *104*, 7847.

(8) (a) Klotz, B.; Barnes, I.; Golding, B. T.; Becker, K. H. *Phys. Chem. Chem. Phys.* **2000**, *2*, 227. (b) Klotz, B.; Barnes, I.; Becker, K. H.; Golding, B. T. J. *Chem. Soc., Faraday Trans.* **1997**, *93*, 1507.

(9) Zhao, J.; Zhang, R.; Misawa, K.; Shibuya, K. J. *Photochem. Photobiol. A: Chem.* **2005**, *176*, 199.

(10) Kassaee, M. Z.; Arshadi, S.; Ahmadi-Taheri, N. *J. Mol. Struct. (THEOCHEM)* **2005**, *715*, 107.

(11) (a) Raoult, S.; Rayez, M-T.; Rayez, J-C.; Lesclaux, R. *Phys. Chem. Chem. Phys.* **2004**, *6*, 2245. (b) Raoult, S. Ph.D. Thesis, University of Bordeaux, 2003.

(12) Frankcombe, T. J.; Smith, S. C. *J. Phys. Chem. A* **2007**, *111*, 3686.

(13) Yu, J.; Jeffries, H. *Atmos. Environ.* **1997**, *31*, 2281

(14) Lynch, J.; Fast, P. L.; Harris, M.; Truhlar, D. G. *J. Phys. Chem. A* **2000**, *104*, 4812.

(15) Cartas-Rosado, R.; Ruíz Santoyo, M.; Alvarez-Idaboy, J. R.; Vivier-Bunge, A. *J. Phys. Chem. A* **2001**, *105*, 9222.

(16) Becke, A. D. *J. Chem. Phys.* **1993**, *98*, 1372.

(17) Lynch, B. J.; Truhlar, D. G. *J. Phys Chem A* **2001**, *105*, 2936.

(18) Frisch, M. J.; Trucks, G. W.; Schlegel, H. B.; Scuseria, G. E.; Robb, M. A.; Cheeseman, J. R.; Montgomery, J. A., Jr.; Vreven, T.; Kudin, K. N.; Burant, J. C.; Millam, J. M.; Iyengar, S. S.; Tomasi, J.; Barone, V.; Mennucci, B.; Cossi, M.; Scalmani, G.; Rega, N.; Petersson, G. A.; Nakatsuji, H.; Hada, M.; Ehara, M.; Toyota, K.; Fukuda, R.; Hasegawa, J.; Ishida, M.; Nakajima, T.; Honda, Y.; Kitao, O.; Nakai, H.; Klene, M.; Li, X.; Knox, J. E.; Hratchian, H. P.; Cross, J. B.; Bakken, V.; Adamo, C.; Jaramillo, J.; Gomperts, R.; Stratmann, R. E.; Yazyev, O.; Austin, A. J.; Cammi, R.; Pomelli, C.; Ochterski, J. W.; Ayala, P. Y.; Morokuma, K.; Voth, G. A.; Salvador, P.; Dannenberg, J. J.; Zakrzewski, V. G.; Dapprich, S.; Daniels, A. D.; Strain, M. C.; Farkas, O.; Malick, D. K.; Rabuck, A.

D.; Raghavachari, K.; Foresman, J. B.; Ortiz, J. V.; Cui, Q.; Baboul, A. G.; Clifford, S.; Cioslowski, J.; Stefanov, B. B.; Liu, G.; Liashenko, A.; Piskorz, P.; Komaromi, I.; Martin, R. L.; Fox, D. J.; Keith, T.; Al-Laham, M. A.; Peng, C. Y.; Nanayakkara, A.; Challacombe, M.; Gill, P. M. W.; Johnson, B.; Chen, W.; Wong, M. W.; Gonzalez, C.; Pople, J. A. *Gaussian 03*, revision D.01; Gaussian, Inc.: Wallingford, CT, 2004.

(19) (a) Uc, V. H.; Alvarez-Idaboy, J. R.; Galano, A.; García-Cruz, I.; Vivier-Bunge, A. *J. Phys. Chem. A* **2006**, *110*, 10155. (b) Pilling, M. J.; Seakins, P. W. *Reaction Kinetics*; Oxford University Press: New York, 1996.

(20) (a) Günther, H.; Schubarth, R.; Vogel, Z. E. *Naturforsch., B* **1967**, *22*, 25. (b) Vogel, E.; Günther, H. *Angew. Chem.* **1967**, *79*, 429.

(21) Sosa, C.; Schlegel, H. B. *J. Am. Chem. Soc.* **1987**, *109*, 4193.

(22) Díaz-Acosta, I.; Alvarez-Idaboy, J. R.; Vivier-Bunge, A. *I. J. Chem. Kinet.* **1999**, *31*, 29.

(23) Alvarez-Idaboy, J. R.; Mora-Diez, N.; Boyd, R. J.; Vivier-Bunge, A. *J. Am. Chem. Soc.* **2001**, *123*, 2018.

(24) Smith, I. W. M.; Ravishankara, A. R. *J. Phys Chem A* **2002**, *106*, 4798.

(25) Ayala, P. Y.; Schlegel, H. B. *J. Chem. Phys.* **1998**, *108*, 2314.